

Article

Real-Time Analysis of Individual Ebola Virus Glycoproteins Reveals Pre-Fusion, Entry-Relevant Conformational Dynamics

Natasha D. Durham ^{1,2,*}, Angela R. Howard ^{2,†}, Ramesh Govindan ^{1,2,†}, Fernando Senjobe ², J. Maximilian Fels ³, William E. Diehl ⁴, Jeremy Luban ⁴, Kartik Chandran ³ and James B. Munro ^{1,2,*}

¹ Department of Microbiology and Physiological Systems, University of Massachusetts Medical School, Worcester, MA 01605, USA; ramesh.govindan@tufts.edu

² Department of Molecular Biology and Microbiology, Tufts University School of Medicine and Sackler School of Graduate Biomedical Sciences, Boston, MA 02111, USA; angela.howard@tufts.edu (A.R.H.); senjobe@g.harvard.edu (F.S.)

³ Department of Microbiology and Immunology, Albert Einstein College of Medicine, Bronx, NY 10461, USA; max.fels@gmail.com (J.M.F.); kartik.chandran@einstein.yu.edu (K.C.)

⁴ Program in Molecular Medicine, University of Massachusetts Medical School, Worcester, MA 01605, USA; william.diehl@umassmed.edu (W.E.D.); jeremy.luban@umassmed.edu (J.L.)

* Correspondence: natasha.durham@umassmed.edu (N.D.D.); james.munro@umassmed.edu (J.B.M.)

† These authors contributed equally to this work.

Received: 16 December 2019; Accepted: 10 January 2020; Published: 15 January 2020



Abstract: The Ebola virus (EBOV) envelope glycoprotein (GP) mediates the fusion of the virion membrane with the membrane of susceptible target cells during infection. While proteolytic cleavage of GP by endosomal cathepsins and binding of the cellular receptor Niemann-Pick C1 protein (NPC1) are essential steps for virus entry, the detailed mechanisms by which these events promote membrane fusion remain unknown. Here, we applied single-molecule Förster resonance energy transfer (smFRET) imaging to investigate the structural dynamics of the EBOV GP trimeric ectodomain, and the functional transmembrane protein on the surface of pseudovirions. We show that in both contexts, pre-fusion GP is dynamic and samples multiple conformations. Removal of the glycan cap and NPC1 binding shift the conformational equilibrium, suggesting stabilization of conformations relevant to viral fusion. Furthermore, several neutralizing antibodies enrich alternative conformational states. This suggests that these antibodies neutralize EBOV by restricting access to GP conformations relevant to fusion. This work demonstrates previously unobserved dynamics of pre-fusion EBOV GP and presents a platform with heightened sensitivity to conformational changes for the study of GP function and antibody-mediated neutralization.

Keywords: Ebola virus; envelope glycoprotein; conformational dynamics; single-molecule FRET; virus entry

1. Introduction

Ebola virus (EBOV) disease outbreaks in West and Sub-Saharan Africa have occurred since the emergence of the virus in 1976 [1]. The 2014–2016 West African outbreak resulted in more than 28,000 cases and 11,000 fatalities, and the current outbreak in the Democratic Republic of Congo continues to claim lives. The most promising vaccine and therapeutic target for EBOV infection is the envelope glycoprotein (GP), which coordinates viral-host membrane fusion. GP exists as a trimer of GP1–GP2 heterodimers which resides on the surface of the EBOV virion [2]. GP1 mediates virus attachment and

receptor binding, and GP2 promotes membrane fusion. Following attachment to the cell surface, EBOV is trafficked to late endosomes where GP1 is proteolytically cleaved by host cathepsins to remove the mucin-like domain (muc) and the glycan cap, forming GP_{CL} [3,4]. This cleavage event exposes the binding site for the host receptor for EBOV, Niemann-Pick C1 protein (NPC1). Binding of GP_{CL} to the luminal domain C of NPC1 (NPC1-C) is necessary, but not sufficient, to trigger GP-mediated fusion of the viral and endosomal membranes [5–9]. As the sole surface antigen of EBOV, GP is also the target of host neutralizing antibodies (nAbs), which may function to inhibit conformational changes required for membrane fusion [10].

Atomic resolution structures of the pre-fusion mucin-deleted, transmembrane (TM)-deleted GP ectodomain (GP Δ TM) in unliganded and antibody-bound states depict a conformation in which the fusion loop of GP2 is sequestered in a hydrophobic cleft, which spans the interface of two neighboring protomers [2,11–13]. Structures of uncleaved GP and GP_{CL} in complex with NPC1-C depict similar global conformations of the GP2 fusion loop with respect to GP1 [14,15]. In contrast, structures of post-fusion GP2 fragments indicate a loop-to-helix transition in the heptad repeat 1 (HR1) region of GP2, which would translate the fusion loop away from the surface of the virion and toward the target membrane, similar to that described for influenza hemagglutinin [16]. In the post-fusion conformation of GP, HR1 ultimately forms a single helix antiparallel to HR2 [17,18]. Thus, structural models indicate the endpoint conformations that GP adopts during membrane fusion, implying that GP is capable of undergoing large-scale conformational changes. However, direct evidence for the trajectory connecting the pre- and post-fusion conformations, including the significance of GP cleavage and NPC-1 binding in promoting this conformational rearrangement, is currently lacking.

Here, we sought to visualize the conformational dynamics of GP during the steps preceding membrane fusion. We first designed a single-molecule Förster resonance energy transfer (smFRET) imaging approach to detect real-time changes in the conformation of the trimeric GP ectodomain (GP Δ TM), as well as functional, pseudovirus-associated GP (GP Δ muc) with an intact transmembrane domain. We found that both GP Δ TM and GP Δ muc are intrinsically dynamic. GP Δ TM exhibits a predominant conformational state that is consistent with existing structures determined by x-ray [2,11]. This conformation is also sampled by pseudovirion-associated GP Δ muc. Removal of the glycan cap of GP Δ muc and NPC1 binding destabilize the conformation depicted by crystallography, suggestive of promotion of conformations on pathway to fusion. Thus, glycan cap removal may play an active role in promoting EBOV entry beyond exposing the receptor-binding site. Finally, we also find that neutralizing antibodies bound to GP Δ muc enrich for alternative conformations, thus destabilizing access to this entry-relevant conformation, which may thereby block virus entry.

2. Materials and Methods

2.1. Cell Lines

HEK293T cells (American Type Culture Collection, Manassas, VA, USA; ATCC) were maintained at 37 °C and 5% CO₂ in DMEM complete, consisting of Dulbecco's Modified Eagle medium (DMEM; ThermoFisher, Waltham, MA, USA) with 10% BenchMark Fetal Bovine Serum (Gemini Bio-Products, West Sacramento, CA, USA), 1% L-Glutamine (Thermo Fisher, Waltham, MA, USA), and 1% penicillin-streptomycin (Thermo Fisher, Waltham, MA, USA). FreeStyle 293-F cells (Thermo Fisher, Waltham, MA, USA) were cultured in FreeStyle 293 Expression Medium (Thermo Fisher, Waltham, MA, USA) at 37 °C and 8% CO₂.

2.2. Plasmids

The EBOV GP Δ muc Mayinga variant (Genbank accession number NP_066246) was used in all pseudoparticle experiments. GP Δ muc lacks residues 309–489 corresponding to the mucin-like domain. EBOV GP Δ TM is a derivative of the GP Δ muc Mayinga variant with deletions of residues 313–463 of the mucin domain and residues 633–676 of the transmembrane domain, and encodes a C-terminal

foldon trimerization peptide and 6X His tag. For single-molecule FRET experiments, GP Δ TM and GP Δ muc were modified such that the nucleotide sequence encoding A1 and A4 peptides were inserted at the N-terminal positions of GP1 and GP2, respectively. A1 was inserted between amino acid 32 and 33 of GP1 (Figure 1b). A4 was inserted between amino acid 501 and 502 of GP2 (Figure 1b). pNL4.3R-E (NIH AIDS Reagent Program, Division of AIDS, NIAID, NIH from Dr. Nathaniel Landau) was used to generate retroviral pseudoparticles, as described below. Plasmids encoding luminal domain C of NPC1 [6], and KZ52 [19] have been previously described.

2.3. Protein Production and Purification

Soluble NPC1-C containing an N-terminal FLAG and 6X His tag were produced by transfection in FreeStyle 293-F cells (Thermo Fisher, Waltham, MA, USA) with polyethyleneimine (PEI MAX, Polysciences, Warrington, PA, USA). Six days post-transfection, cell culture supernatant containing soluble protein was harvested and purified using PerfectPro Ni-NTA Agarose beads (PRIME GmbH, Neuss, Germany). Purified NPC1-C was dialyzed 20 mM Tris-HCl, 100 mM NaCl, 2 mM 2-mercaptoethanol, and 10% glycerol and concentrated in Vivaspin 6 ultracentrifugation spin columns (Sartorius, Gottingen, Germany). NPC1-C was stored at -80°C prior to use. KZ52 was produced by transfection of plasmids encoding heavy and light chains into FreeStyle 293-F cells with PEI. At 3 days post-transfection, the cell culture supernatant was collected and replaced with fresh medium. The supernatant was collected again at 6 days post-transfection. The 3- and 6-day supernatant fractions were pooled, and KZ52 antibody was extracted using standard protein A affinity chromatography. After eluting from protein A in 0.2 M citric acid pH3, KZ52 was dialyzed into PBS and stored at -80°C prior to use. GP Δ TM was produced as described below.

2.4. Infectivity and Neutralization Assays

Retroviral pseudoparticles were generated with all tagged GP Δ muc 32-A1/501-A4 or all wild-type GP Δ muc by transfection of HEK293T cells with Lipofectamine 3000 Reagent (Thermo Fisher, Waltham, MA, USA) at 1:5 GP-encoding plasmid:pNL4-3.R-E- backbone. Virus was harvested 48 h after transfection, concentrated 10- or 20-fold with Lenti-X Concentrator (Clontech, Mountain View, CA, USA) and resuspended in DMEM complete. The infectivity or neutralization of retroviral pseudovirions was determined by Firefly Luciferase reporter gene activity using the Luciferase Assay System (Promega, Madison, WI, USA). HEK293T cells were seeded 24 h before infection in an opaque 96-well clear bottom white microplate (Thermo Fisher, Waltham, MA, USA). For infectivity assays, cells were infected directly with pseudovirions. For neutralization assays, virus was incubated with 15 $\mu\text{g}/\text{mL}$ of antibody (unless otherwise stated) at 37°C for 30 min before addition of the virus-antibody mixture to cells. Cell culture media was replaced 24 h after infection. 48 h post-infection, cells were washed with PBS (Thermo Fisher, Waltham, MA, USA), lysed with Cell Culture Lysis Reagent (Promega, Madison, WI, USA) and firefly luciferase reporter gene activity was detected using a Synergy H1 microplate reader (BioTek Instruments, Winooski, VT, USA). Infectivity of rVSV-GP Δ muc was assayed as previously described [3].

2.5. sNPC1-C ELISA

Pseudovirions were produced as described above by co-transfection of plasmids encoding HIV-1 backbone and either GP Δ muc or GP Δ muc 32-A1/501-A4, at a 1:1 ratio. Immediately before use, pseudoparticles were concentrated and treated for 1 h at 37°C with 0.25 mg/mL thermolysin (Promega, Madison, WI, USA) in 50 mM Tris-HCl pH8, 0.5 mM CaCl_2 . The uncleaved control was incubated in the same way in the absence of thermolysin. Reactions were terminated with EDTA. ELISAs to determine NPC1-C binding to GP Δ muc or GP CL were preformed based on previously published methods [6,20]. Briefly, high-binding 96-well ELISA plates (Thermo Fisher, Waltham, MA, USA) were coated with concentrated pseudoparticles diluted in PBS. Plates were blocked with 2% milk containing 3% bovine serum albumin in PBS. Unbound virus was washed off and 10-fold dilutions of NPC1-C (0–40 $\mu\text{g}/\text{mL}$)

were added. Bound NPC1-C was detected with the horseradish peroxidase-conjugated anti-FLAG antibody (Millipore Sigma, Burlington, MA, USA) followed by Ultra-TMB substrate (Thermo Fisher, Waltham, MA, USA). All incubations were performed for 1 h at 37 °C.

2.6. Immunoblots

Denatured samples containing pseudovirions were run on 10% polyacrylamide gels (Millipore Sigma, Burlington, MA, USA) and transferred to nitrocellulose membranes. Membranes were blocked overnight at 4 °C. The mAb H3C8 [21] was used to detect GP and GP_{CL}, and the mAb B1217M (GeneTex, Irvine, Ca, USA) to detect the HIV-1 structural protein p24. All primary antibodies were detected with a horseradish peroxidase-conjugated rabbit anti-mouse IgG Fc (Thermo Fisher, Waltham, MA, USA).

2.7. GP Δ TM Production and Labeling for smFRET Imaging

GP Δ TM was produced by transfection in FreeStyle 293-F cells (Thermo Fisher, Waltham, MA, USA) with polyethylenimine (PEI MAX, Polysciences, Warrington, PA, USA). Wild-type GP Δ TM and GP Δ TM 32-A1/501-A4 expression constructs were co-transfected at a ratio of 2:1. At 6 days post-transfection, cell culture supernatant containing soluble protein was harvested and purified using PerfectPro Ni-NTA Agarose beads (PRIME GmbH, Neuss, Germany). Purified GP Δ TM was exchanged into PBS supplemented with 10mM MgOAc using Vivaspin 6 ultracentrifugation spin columns (Sartorius, Gottingen, Germany) and then incubated overnight at room temperature with 5 μ M each of fluorophores LD550 and LD650 (Lumidyne Technologies, New York, NY, USA) conjugated to coenzyme A (CoA; Millipore Sigma, Burlington, MA, USA) and 5 μ M of the labeling enzyme AcpS. Labeled protein was purified away from free dye and enzyme via size exclusion chromatography, on a Superdex 200 Increase 10/300 GL column (GE Healthcare, Chicago, IL, USA) in PBS. Fractions containing GP Δ TM were pooled and concentrated to 1–2 mg/mL. Aliquots were flash-frozen in liquid nitrogen and stored at –80 °C until use.

2.8. Pseudovirus Production and Labeling for smFRET Imaging

Retroviral pseudoparticles containing a single fluorescently labeled GP protomer per virion were generated by transfection of HEK293T cells with Lipofectamine 3000 Reagent (Thermo Fisher, Waltham, MA, USA) at a 5:1 ratio of pNL4-3R-E- over plasmid encoding GP. Plasmid encoding GP consisted of a 50:1 mixture of plasmid encoding wild-type GP Δ muc:GP Δ muc 32-A1/501-A4. Virus was harvested 48 h after transfection, concentrated and labeled with fluorophores as described [22]. Briefly, harvested virus was concentrated by ultracentrifugation through a 10% sucrose cushion for 2 h at 25,000 \times g, resuspended in labeling buffer (50 mM HEPES pH 7.5, 10 mM MgOAc) and incubated overnight with 0.5 μ M each of fluorophores LD550-CoA and LD650-CoA and 5 μ M of the labeling enzyme AcpS. To facilitate surface-immobilization of labeled virions for imaging, DSPE-PEG2000-biotin (Avanti Polar Lipids, Alabaster, AL, USA) lipid was added to samples and incubated at room temperature for 30 min. Labeled virus was purified from unbound fluorophores and lipid by ultracentrifugation through a 6–30% OptiPrep (Millipore Sigma, Burlington, MA, USA) density gradient for 1 h at 35,000 \times g, and virus-containing fractions were identified by immunoblot for GP and p24.

2.9. smFRET Imaging

Purified and labeled GP Δ TM or pseudovirus was immobilized and imaged using wide-field prism-based TIRF, as described [23]. smFRET data were acquired at room temperature using Metamorph software (Molecular Devices, San Jose, CA, USA) for 40 s at 25 frames/s. To generate pseudovirions containing GP_{CL}, virus was treated with thermolysin as described above, terminated with phosphoramidon, and either imaged immediately or incubated with 1.7 μ M (80 μ g/mL) purified NPC1-C for 30 min at room temperature immediately prior to surface immobilization and imaging. For conditions containing monoclonal antibody, the indicated antibody was diluted in imaging buffer and incubated with surface immobilized pseudovirions for 30 min at room temperature immediately prior

to imaging. KZ52 was prepared as described above. Purified c2G4 and c4G7 were provided by Mapp Biopharmaceutical (San Diego, CA, USA). Purified ADI-15946, ADI-15878, ADI-15742, ADI-15750, and ADI-16061 were provided by Adimab (Lebanon, NH, USA).

2.10. Analysis of smFRET Data

All smFRET data was processed and analyzed using the SPARTAN software package (<https://www.scottblanchardlab.com/software>) in Matlab (Mathworks, Natick, MA, USA) [24]. smFRET trajectories were identified according to four criteria: (i) exceeded a minimum total fluorescence intensity; (ii) duration of smFRET trajectory exceeded 15 frames; (iii) correlation coefficient calculated from the donor and acceptor fluorescence trajectories was less than -0.1 ; and (iv) signal-to-noise ratio was greater than 8. Due to greater heterogeneity in the smFRET data acquired on pseudovirion-associated GP, trajectories that passed these criteria were then verified manually. Hidden Markov model (HMM) selection was performed using the Baum-Welch algorithm, with correction of the maximized log-likelihood for different numbers of model parameters using the Akaike information criterion (AIC) [25]. smFRET trajectories were idealized to the determined model using the segmental k-means algorithm [26] implemented in SPARTAN.

2.11. Molecular Dynamics Simulation of Fluorescently Labeled GP Δ TM

Atomic coordinates were obtained from a structure of GP Δ TM determined by X-ray crystallography (PDB accession 5JQ3) [11]. Amino acids corresponding to the A1 (GDSLDMLEWSLM) and A4 (DSLDMLEW) peptides were attached to the N termini of GP1 and GP2, respectively in PyMol (version 2.3.1, Schrödinger, Cambridge, MA, USA). Atomic models of LD550- and LD650-maleimide with a phosphopantetheinyl linker were constructed in PyMol (version 2.3.1, Schrödinger, Cambridge, MA, USA). The fluorophore geometries were initially optimized at the AM1 level of theory with the sqm program in AmberTools (version 16, San Francisco, CA, USA). The geometries were further optimized, and the electrostatic potential (ESP) calculations were performed at the HF/6-31G (d) level of theory in Gaussian 9 (Gaussian, Inc., Wallingford, CT, USA). Partial atomic charges were then derived by restrained electrostatic potential (RESP) fitting using antechamber in AmberTools. Atom types and bonded parameters from the Generalized Amber Force Field (GAFF2) were assigned using antechamber and parmchk2 in AmberTools. The fluorophores and linkers were attached at the serine residue at positions 3 and 2 of the A1 and A4 peptides, respectively in LEaP. The protein component of the system was parameterized with the Amber force field (ff14SB). The entire system was charge-neutralized and solvated in explicit water using the TIP3P model with periodic boundary conditions in LEaP. The system was energy minimized for 0.1 ns, followed by a 50 ns simulation run in the NPT ensemble, with temperature and pressure maintained at 300 K and 1 atm through the use of Langevin dynamics and the Nose'-Hoover Langevin piston method, respectively. Simulations were run using NAMD (version 2.12, Urbana-Champaign, IL, USA) on the Tufts Research Cluster.

3. Results

3.1. Site-Specific Fluorescent Labelling of EBOV GP

The application of smFRET imaging requires site-specific attachment of donor and acceptor fluorophores to GP. We specifically sought to probe movement of GP1 with respect to GP2, as well as movement of the viral fusion loop that is proximal to the N terminus of GP2. Both motions are predicted to be critical to the mechanism of GP-mediated membrane fusion [16]. To this end, we modified GP Δ TM from the Mayinga strain of EBOV for the site-specific attachment of donor and acceptor fluorophores (Figure 1a). This construct contained deletions of the mucin domain and transmembrane domain, and included a foldon trimerization peptide and C-terminal 6X His tag, similar to that characterized by x-ray crystallography but with residue T at position 42 to maintain the native glycosylation site [11]. We inserted the 12-residue A1 peptide into the N terminus of GP1, and the 8-residue A4 peptide into

the N-terminus of GP2 to generate GP Δ TM 32-A1/501-A4 (Figure 1b,c). These peptide tags enable enzymatic attachment of fluorophore conjugates to a specific serine residue within each peptide [27,28]. Molecular dynamics simulation of GP Δ TM in the pre-fusion conformation with the peptide tags and conjugated fluorophores suggested an inter-fluorophore distance of approximately 30 Å, predictive of high FRET (Figure 1c).

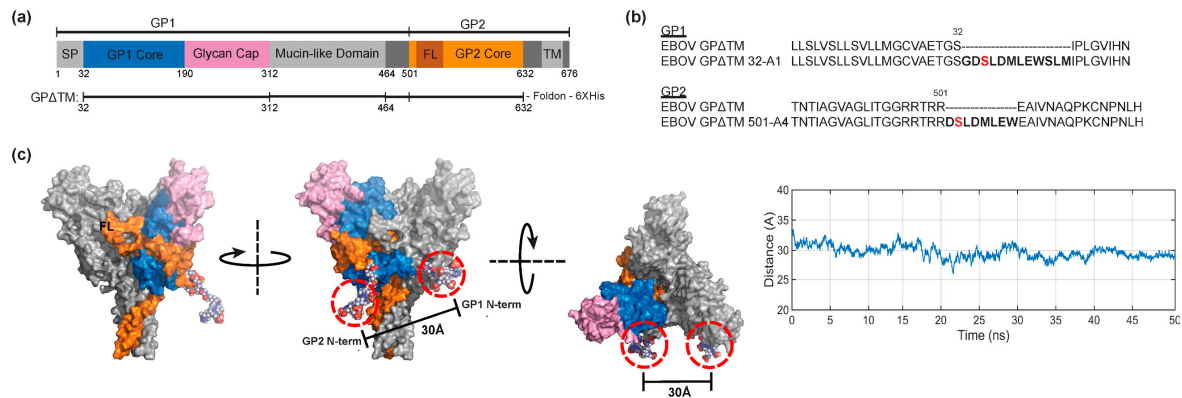


Figure 1. Site-specific fluorescent labelling of EBOV GP for smFRET. (a) Structural organization of GP Δ TM. Adapted from Ref. [11]. FL, fusion loop; SP, signal peptide; TM, transmembrane helix. (b) EBOV GP Δ TM and GP Δ muc were modified to contain peptide tags (bold) in GP1, between amino acid position 32 and 33, and in GP2, between amino acid positions 501 and 502, to facilitate enzymatic labelling with fluorophores at the serine residues highlighted in red. (c) Surface rendering of EBOV GP Δ TM (derived from PDB accession 5JQ3 [11]) with fluorophores attached. MD simulation of fluorescently labeled GP Δ TM 32-A1/501-A4 predicts an inter-fluorophore distance of approximately 30 Å. After minimization and equilibration, the time-averaged distance between the centers of mass of the fluorophores was determined through a 50-ns simulation (see Section 2).

We next verified that these peptide-insertion sites did not disrupt GP function by creating analogous insertions in full-length, transmembrane-intact GP Δ muc (i.e., GP Δ muc 32-A1/501-A4). When expressed either GP Δ muc 32-A1/501-A4 or untagged GP Δ muc on pseudovirions using a recombinant vesicular stomatitis virus (rVSV) core that encodes GFP [24]. Pseudovirions containing GP Δ muc 32-A1/501-A4 maintained infectivity levels comparable to those bearing untagged GP Δ muc (Figure 2a). Since the low density of glycoproteins on the surface of retroviral particles provides the best platform for smFRET imaging, we formed HIV-1 particles pseudotyped with GP Δ muc 32-A1/501-A4 and characterized incorporation into virus particles, cleavage of the glycan cap by thermolysin, sensitivity to neutralization by a panel of antibodies, and NPC1-C binding (Figure 2b–d). In all cases, pseudovirion-associated GP Δ muc 32-A1/501-A4 maintained phenotypes comparable to wild-type GP Δ muc.

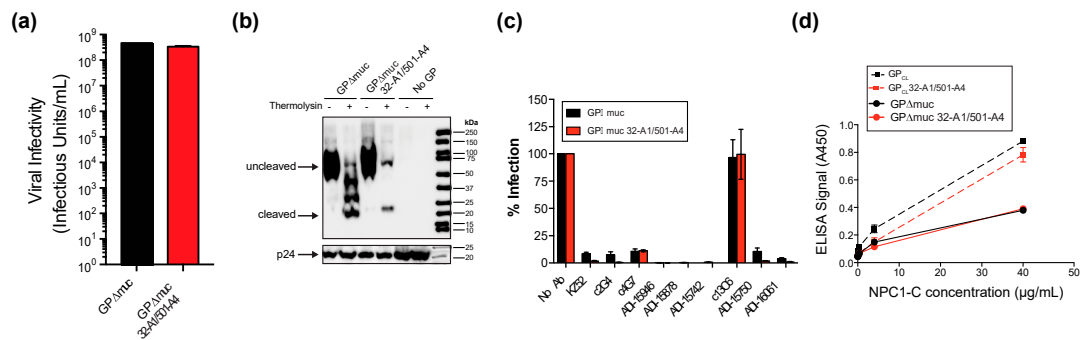


Figure 2. Characterization of pseudovirions containing peptide tags for site-specific fluorophore attachment. **(a)** Infectivity of pseudovirions containing either GP Δ muc or GP Δ muc 32-A1/501-A4 using a recombinant vesicular stomatitis virus (VSV) core that encodes GFP. Viral infectivity was determined by counting eGFP-positive Vero cells 14–16 h post infection. Results are shown as the mean \pm standard error ($n = 3$). **(b)** Western blot of retroviral pseudovirions containing GP Δ muc, GP Δ muc 32-A1/501-A4 or no GP after 1 h mock treatment (–) or treatment with thermolysin (+) to cleave the glycan cap and generate GP Δ CL. The HIV structural protein p24 indicates the total amount of virus loaded. **(c)** Neutralization of retroviral pseudoparticles by monoclonal antibodies. Antibodies were tested at 15 μ g/mL for neutralizing activity against retroviral pseudoparticles containing either GP Δ muc (black bars) or GP Δ muc 32-A1/501-A4 (red bars). Luciferase activity was detected 48 h post-infection and expressed as a percentage of infection with no antibody (No Ab). Results are shown as the mean \pm standard error ($n = 2$). **(d)** ELISA for NPC1-C binding to retroviral pseudovirions containing only GP Δ muc or GP Δ muc 32-A1/501-A4, with or without thermolysin treatment to generate GP Δ CL or GP Δ CL 32-A1/501-A4. Results are shown as the mean \pm standard error ($n = 3$).

3.2. Conformational Dynamics of EBOV GP Δ TM

To generate trimeric protein for smFRET imaging, 293-Freestyle cells were co-transfected with plasmids encoding GP Δ TM 32-A1/501-A4 and untagged GP Δ TM at a ratio of 1:2 (Section 2). This was found to optimize the proportion of GP Δ TM trimers containing a single GP Δ TM 32-A1/501-A4 protomer. smFRET measurements could then be made that originated from a single donor-acceptor fluorophore pair on the same GP Δ TM protomer (Figure 3a), as previously described for studies of other envelope glycoproteins on the surface of virions [22,23]. Trimers containing enzymatically attached fluorophores were surface immobilized and imaged by prism-based total internal reflection fluorescence (TIRF) microscopy (Section 2) (Figure 3a). We confirmed by western blot that the sample of GP Δ TM used in smFRET imaging contained minimal amounts of GP0 and remained intact during protein expression and purification (Figure 3b). We observed smFRET trajectories indicating intrinsic and spontaneous fluctuations between multiple FRET states during the observation period of approximately 20 s (Figure 3c). Hidden Markov modeling (HMM) indicated a predominant high-FRET state (0.74 ± 0.08) with 52.6% occupancy, as displayed in histograms of the FRET values compiled from the population of observed molecules (Figure 3d, left). This high-FRET state is consistent with the ~ 30 Å inter-fluorophore distance predicted by molecular dynamics simulation of fluorescently labeled GP in the conformation determined by x-ray crystallography (Figure 1c) [2,11,14]. We also observed two additional states, 0.27 ± 0.08 and 0.50 ± 0.08 FRET, suggestive of alternative GP conformations in which the distance between the fluorophore pair increases. The intermediate- and low-FRET states were present with occupancies of 26.9% and 20.5%, respectively (Table 1). A transition density plot (TDP) displays the relative frequencies of observed transitions within this population of trimers. The TDP shows roughly equal transition frequencies between the high- and intermediate-FRET states, and between the intermediate- and low-FRET states; transitions directly between the high- and low-FRET states were rarely seen (Figure 3d, right). The TDP is symmetric about the diagonal axis, which indicates equilibrium dynamics between multiple states. These data suggest that pre-fusion GP Δ TM

is intrinsically dynamic, sampling two conformations in addition to that which has been described by crystallography.

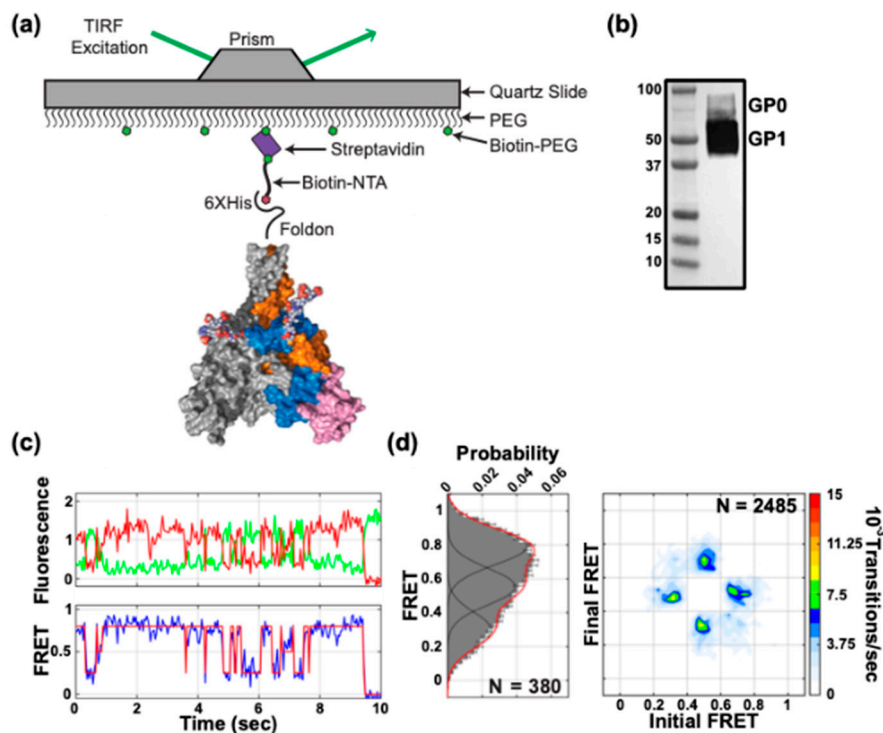


Figure 3. Conformational dynamics of EBOV GP Δ TM. (a) smFRET imaging of GP Δ TM trimers containing a single fluorescently-labelled protomer within an otherwise wild-type GP Δ TM trimer were surface-immobilized via biotin-NTA on a streptavidin-coated quartz microscope slide for smFRET imaging with TIRF microscopy. (b) Western blot of purified GP Δ TM used in smFRET imaging using an anti-GP1 antibody (H3C8). (c) Representative fluorescence trace (top) showing fluorescence intensity over time for a donor (LD550; green) and acceptor (LD650; red) fluorophore pair on a single GP Δ TM trimer, and the corresponding FRET trajectory (bottom). Overlaid on the FRET trajectory is the idealization (red) resulting from HMM analysis. (d) (Left) Population FRET histogram for GP Δ TM trimers composed of FRET trajectories summed over the observation window. Overlaid on the histograms are Gaussian distributions with means 0.3, 0.5 and 0.7 that reflect the results of HMM analysis. N indicates the number of trimers in the population histogram. (Right) Transition density plot (TDP) displaying the relative frequencies of observed transitions generated from idealizations of individual FRET trajectories. N indicates the total number of transitions within the population of trimers analyzed.

Table 1. Förster resonance energy transfer (FRET) state occupancies determined through hidden Markov modeling.

	Occupancies (%)		
	Low FRET	Intermediate FRET	High FRET
GP Δ TM	20.5%	26.9%	52.6%
GP Δ muc	31.4%	23.6%	45.0%
GP _{CL}	22.2%	45.8%	32.0%
GP _{CL} + NPC1-C	19.8%	53.4%	26.8%
GP Δ muc + KZ52 (15 μ g/mL)	35.7%	23.3%	41.0%
GP Δ muc + KZ52 (500 μ g/mL)	42.0%	23.2%	34.8%
GP Δ muc + c2G4	46.7%	24.9%	28.4%
GP Δ muc + c4G7	47.2%	25.6%	27.2%

Table 1. Cont.

	Occupancies (%)		
	Low FRET	Intermediate FRET	High FRET
GP Δ muc + ADI-15946	27.1%	25.0%	47.9%
GP Δ muc + ADI-15878	20.8%	20.2%	59.0%
GP Δ muc + ADI-15742	21.8%	23.3%	49.3%
GP Δ muc + ADI-15750	41.4%	23.6%	35.0%
GP Δ muc + ADI-16061	32.0%	23.1%	44.9%

3.3. Conformational Dynamics of Pseudovirion-Associated EBOV GP Δ muc

We next asked whether the dynamics observed for GP Δ TM are representative of full-length functional GP Δ muc. We therefore transferred the same fluorophore attachment strategy to GP Δ muc on the surface of retroviral pseudovirions. As done previously for influenza hemagglutinin and HIV Env [22,23], we formed pseudovirions with the HIV core and an excess of wild-type GP Δ muc over GP Δ muc 32-A1/501-A4 (Section 2). This dilution of GP Δ muc 32-A1/501-A4 with wild-type GP Δ muc maximized the probability that only a single fluorophore pair was present on the surface of each virion (Figure 4a). Similar to the data for GP Δ TM, we observed smFRET trajectories indicating intrinsic and spontaneous fluctuations between multiple FRET states (Figure 4b). Notably, HMM analysis of the smFRET trajectories revealed the same low- (0.28 ± 0.07), intermediate- (0.50 ± 0.08) and high- (0.73 ± 0.08) FRET states as observed for GP Δ TM (Figure 3c,d). However, we observed lower intrinsic occupancy of the high-FRET state, higher occupancy in the low-FRET state, and slightly lower occupancy of the intermediate-FRET state as compared to GP Δ TM (Table 1). The TDP indicates that transitions occur between all three FRET states, with transitions between high and intermediate FRET, and between intermediate and low FRET being most frequent (Figure 4b). These data suggest that pre-fusion, unliganded GP Δ muc, similarly to GP Δ TM, can spontaneously and reversibly transition between multiple conformations on the surface of pseudovirions.

3.4. Effects of Proteolytic Cleavage and NPC1 Binding on EBOV GP Δ muc Conformation

We next examined whether proteolytic removal of the glycan cap and subsequent binding to soluble NPC1-C (sNPC1-C) induce conformational changes in GP Δ muc. We treated the pseudovirions with thermolysin to generate GP_{CL} immediately prior to smFRET imaging (Section 2). Individual traces, as well as the population FRET histogram, showed increased occupancy in the intermediate-FRET state for GP_{CL} as compared to GP Δ muc (Figure 4c). Also notable from the TDP was a decrease in the overall level of dynamics, indicated by reduced probability density for all observed transitions. This reflects a reduction in the number of transitions between each FRET state compared to GP Δ muc (Figure 4b). Again, the observed transitions occurred primarily between the intermediate- and high-FRET states and were rarely detected between the low- and high-FRET states. We then asked whether NPC1 binding might further remodel GP conformation. We observed that addition of sNPC1-C to GP_{CL} further promoted an intermediate-FRET state and reduced the occupancy of the low- and high-FRET states (Figure 4d). Equally as dramatic was the reduction in the level of overall dynamics, as depicted in the TDP. These data demonstrated that proteolytic removal of the glycan cap destabilizes the high-FRET conformation preferred by uncleaved GP Δ muc. NPC1 binding further destabilizes this state.

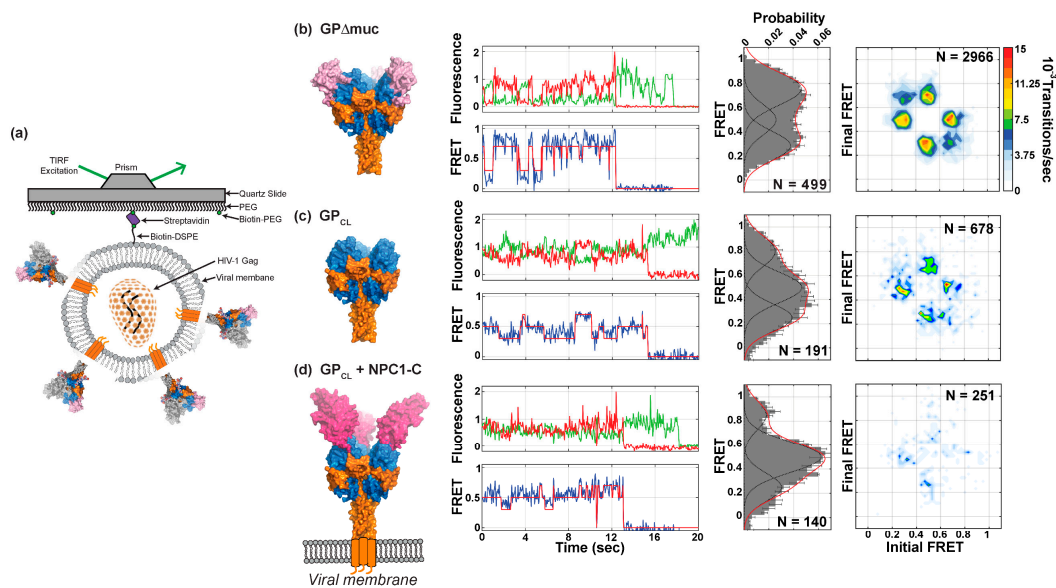


Figure 4. Proteolytic priming and NPC1 binding to EBOV GP Δ muc pseudovirions promote a pre-existing conformation. (a) Pseudovirions containing a single fluorescently labelled protomer within an otherwise native GP Δ muc trimer were surface-immobilized on streptavidin-coated quartz slides for smFRET imaging with TIRF microscopy. (b) (Left) Structure of EBOV GP Δ muc, with subdomains labelled as in Figure 1c. (Left/center) Representative fluorescence trace (top) showing fluorescence intensities over time for a donor (LD550; green) and acceptor (LD650; red) fluorophore pair on a single GP Δ muc on the surface of a pseudovirion. The corresponding FRET trajectory (bottom) is shown in blue. Overlaid on the FRET trajectory is the idealization (red) resulting from HMM analysis. (Right/center) Population FRET histogram for GP Δ muc trimers on pseudovirions composed of FRET trajectories summed over time. Overlaid on the histograms are Gaussian distributions with means 0.3, 0.5, and 0.7 that reflect the results of HMM analysis. N indicates the number of trimers in the population histogram. (Right) TDPs display the relative frequencies of observed transitions, generated from idealizations of individual FRET trajectories for the GP Δ muc population. N indicates the total number of transitions within the population of trimers analyzed. (c) Structural model and smFRET data, displayed as in (b), for GP Δ muc treated with thermolysin to remove the glycan cap (GP_{CL}). (d) Structural models and smFRET data for GP_{CL} bound to sNPC1-C. Structural models were adapted from PDB accessions 5JQ3 and 5F1B [11,14]. Approximate location of the viral membrane is shown.

3.5. Neutralizing Antibodies Mediate GP Conformation

We next asked whether nAbs might function by remodeling GP in a manner that is distinct from proteolytic cleavage and NPC1 binding. In particular, antibodies that interact with GP proximal to the fusion loop are predicted to function by preventing conformational changes necessary for membrane fusion. The antibody KZ52 showed a modest concentration-dependent stabilization of the low-FRET state, which was most pronounced at the saturating concentration of 500 μ g/mL (Figure 5a). This mild effect on GP conformation is consistent with reports of KZ52 incompletely neutralizing EBOV [19,29]; KZ52 may also function by limiting proteolytic cleavage by cathepsins [30]. Additional nAbs were tested at 15 μ g/mL, a concentration that yields minimally 90% neutralization (Figure 2b). The base-binding antibodies c2G4 and c4G7 [31,32] also stabilized the low-FRET state, to a greater extent than KZ52 (Figure 5a). In contrast, ADI-15946, an antibody that competes with KZ52 but bridges the GP1 core and glycan cap [33–35], modestly stabilized the high-FRET state. We also tested nAbs ADI-15878 and ADI-15742, which contact the GP2 fusion loop and adjacent GP1 protomer [33,34,36]. These nAbs significantly increased the occupancy in the high-FRET state (Figure 5b). The glycan-cap binding nAb ADI-15750 slightly stabilized the low-FRET state (Figure 5c) [33]. Finally, the GP2 stalk-binding nAb ADI-16061 (Figure 5d) showed no detectable change in FRET-state occupancy

compared to unliganded GP, indicating that the current fluorophore placement does not report on its mechanism of action [33]. In all cases, transitions to all three FRET states persisted as indicated by the TDPs. Notably, all the nAbs tested stabilized states distinct from proteolytic cleavage and NPC1-C binding. This suggests that their mechanisms of action may be to inhibit transition to the intermediate-FRET conformation.

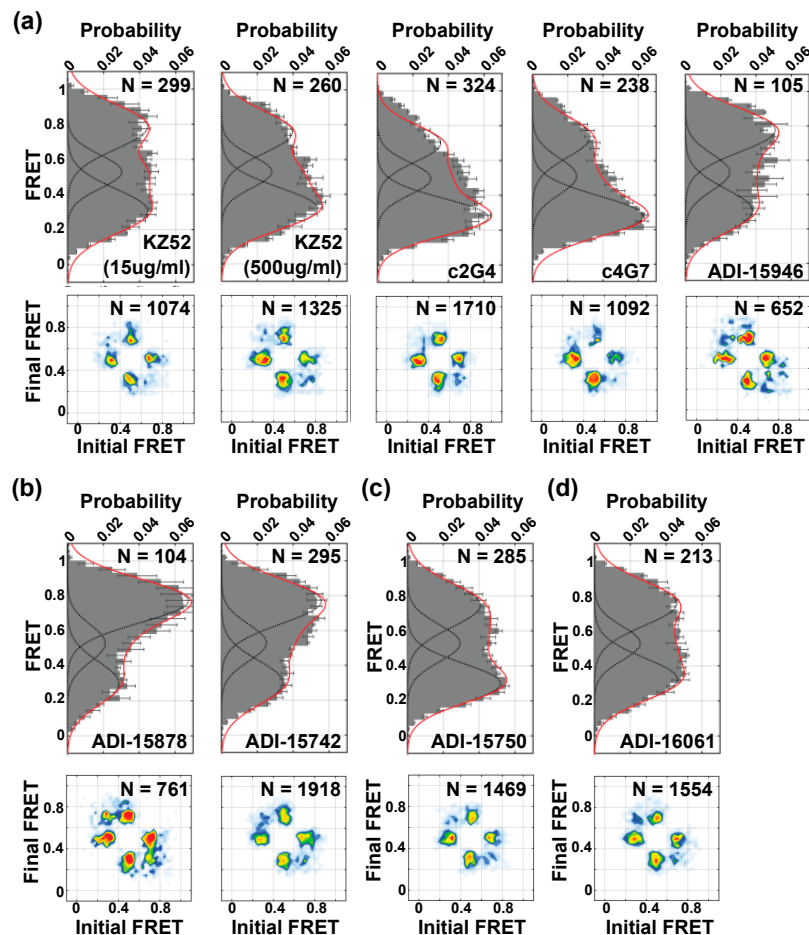


Figure 5. Neutralizing antibodies stabilize distinct EBOV GP Δ mic conformations. Population FRET histograms and corresponding TDPs, displayed as in Figures 3 and 4, for EBOV GP Δ mic in the presence of 15 μ g/mL (unless otherwise noted) of the following: (a) Base-binding antibodies KZ52, c2G4, c4G7, and ADI-15946; (b) base-binding antibodies that contact the GP2 fusion loop and adjacent GP1 protomer ADI-15878 and ADI-15742; (c) Glycan-cap-binding antibody ADI-15750; and (d) GP2 stalk-binding antibody ADI-16061.

4. Discussion

The spring-loaded mechanism of type-I viral fusogens, based largely on studies of influenza hemagglutinin, predicts that dissociation of GP1 from GP2 permits refolding of GP2, which moves the fusion loop toward the target membrane [37]. Structures of pre- and post-fusion GP support this model [2,11,14,18]. The site-specific placement of fluorophores at the N termini of GP1 and GP2 allowed us to visualize movement of the N terminus of GP2, which is proximal to the fusion loop, and the movement of GP1 with respect to GP2. We therefore anticipate that the dynamics observed here reflect conformational changes in GP that relate to its mechanism of membrane fusion. Our approach compliments previous studies of GP by accounting for several key features: (i) real-time changes in GP conformation on the timescale of 10–100 milliseconds; (ii) the use of GP Δ TM as well as GP Δ mic with an intact transmembrane and cytoplasmic region, which permits their direct comparison;

(iii) the functionally relevant context of a viral membrane; and (iv) measurements on single trimers, which precludes the need for averaging measurements from a population of asynchronous trimers. Our results indicate that GP samples multiple conformations beyond what has been described in structural investigations. Molecular modeling supports the identification of the high-FRET state as the conformation depicted in the crystal structures of GP, with the fusion loop positioned in a hydrophobic cleft and contacting the neighboring GP promoter. While the high-FRET state has the highest occupancy for both GP Δ TM and GP Δ muc, our comparison indicates that the presence of the transmembrane domain shifts the conformational equilibrium away from the conformation described by crystallography and favors transition to an alternative conformation.

In order to fully capture the conformational dynamics of complex macromolecules, multiple smFRET signals, stemming from distinct fluorophore attachment strategies are necessary. A parallel study used smFRET imaging with both fluorophores attached to GP2 and was thus insensitive to inter-domain movements [38]. This study indicated no conformational change upon cleavage of the glycan cap. This suggests that the conformational shift toward intermediate FRET seen upon glycan cap cleavage in the present study mainly reflects repositioning of GP1 with respect to GP2. This rearrangement may aid in priming GP1 for interaction with NPC1, and in facilitating other downstream events related to fusion. Recent structural modeling suggests that movement of the fusion loop away from the surface of the virion would require outward motion of GP1, but not necessarily GP1 release, in order to allow the fusion loop access to the space above the GP core [39]. Our results confirm that GP1 does not dissociate from GP2 at this stage, since we still observe reversible transitions into and out of intermediate FRET. Removal of the glycan cap may therefore relieve a physical restriction on the movement of GP2 [40], allowing the fusion loop greater mobility. Das et al. also reported a dramatic repositioning of the GP2 N terminus upon sNPC1-C binding [38]. Thus, the effect of glycan cap cleavage seen in the present study may potentiate GP2 rearrangements promoted by NPC1 binding. The further stabilization of intermediate FRET seen here upon sNPC1-C binding would then reflect additional conformational rearrangements in GP1 and GP2, which result in no detectable change in FRET with the current fluorophore attachment strategy and signal-to-noise ratio. However, when the results of the present study and those of Das et al. are interpreted together, a more complete understanding emerges of the independent effects of glycan cap cleavage and NPC1 binding, respectively. In summary, the current data support the idea that the glycan cap plays an essential role beyond obscuring the receptor-binding site. Specifically, the glycan cap mediates the pre-fusion conformational dynamics of GP, limiting transition to conformations that are putatively on pathway to fusion. An intriguing possibility is that the glycan cap serves to prevent spontaneous triggering of GP prior to arrival of EBOV in the late endosome, at which point the glycan cap is removed by the cellular cathepsins.

In contrast to glycan cap removal and sNPC1-C binding, the nAbs tested here that alter GP conformation either enrich the low-FRET (KZ52, c2G4, and c4G7) or high-FRET (ADI-15878 and ADI-15742) states. We cannot exclude the possibility that base-binding nAbs may cause local changes in the regions of fluorophore attachment. Therefore, it remains possible that the high- and low-FRET states result from local changes in conformation or fluorophore orientation rather than global changes in GP conformation. In either case, these data support the idea that the mechanism of neutralization by these nAbs is to inhibit transition to conformations, such as the intermediate-FRET state, that are relevant to the fusion reaction [10]. At present we cannot rule out the possibility that the neutralizing antibodies enrich for conformations that are distinct from those seen for unliganded and receptor-bound GP, but which are not distinguishable using the current fluorophore placement. The use of additional fluorophore attachment sites in GP1 and GP2, as well as unbiased molecular modeling and structural techniques will further resolve conformations of GP in bound and unliganded states without relying on pre-existing conformations of GP that are favored under conditions of crystal formation. smFRET imaging provides a unique platform for evaluating GP ligands and mutant GP variants that stably present antigenic conformations and should thus find utility in future studies designing novel vaccine candidates and antiviral therapeutics that target GP. Taken together, these observations demonstrate that

the activity of GP in membrane fusion is regulated by ligands that modulate the intrinsic conformational dynamics of GP. smFRET imaging provides a unique platform for evaluating GP ligands and mutant GP variants that stably present antigenic conformations and should thus find utility in future studies designing novel vaccine candidates and antiviral therapeutics that target GP.

Author Contributions: N.D.D., R.G., A.R.H. and J.B.M. designed the research and analyzed the data; N.D.D., A.R.H. and R.G. performed all the experiments unless otherwise stated; F.S. performed ELISAs for NPC1-C binding; J.M.F. performed experiments with VSV pseudovirions; W.E.D., J.L., J.M.F. and K.C. provided reagents and expert feedback; N.D.D., R.G., A.R.H. and J.B.M. wrote the manuscript. All authors contributed to editing of the manuscript. All authors have read and agreed to the published version of the manuscript.

Funding: This work was supported by National Institutes of Health (N.I.H.) grant DP2AI124384 to J.B.M., R01AI134824 to K.C., and DP1DA034990 and R01AI148784 to J.L., A.R.H. was partially supported by N.I.H. grants 2T32AI007422 and 5T32GM007310.

Acknowledgments: The authors thank Larry Zeitlin (Mapp Biopharmaceutical) for providing the ZMapp antibodies, Dennis Burton (Scripps Research Institute) for providing expression plasmids for KZ52, and Carolyn Wilson (FDA) for providing the H3C8 antibody.

Conflicts of Interest: The authors declare no conflict of interest.

References

1. Baseler, L.; Chertow, D.S.; Johnson, K.M.; Feldmann, H.; Morens, D.M. The pathogenesis of Ebola virus disease. *Annu. Rev. Pathol. Mech. Dis.* **2017**, *12*, 387–418. [[CrossRef](#)]
2. Lee, J.E.; Fusco, M.L.; Hessell, A.J.; Oswald, W.B.; Burton, D.R.; Saphire, E. Structure of the Ebola virus glycoprotein bound to an antibody from a human survivor. *Nature* **2008**, *454*, 177–182. [[CrossRef](#)]
3. Chandran, K.; Sullivan, N.; Felbor, U.; Whelan, S.; Cunningham, J. Endosomal proteolysis of the Ebola virus glycoprotein is necessary for infection. *Science* **2005**, *308*, 1643–1645. [[CrossRef](#)] [[PubMed](#)]
4. Schornberg, K.; Matsuyama, S.; Kabsch, K.; Delos, S.; Bouton, A.; White, J. Role of endosomal cathepsins in entry mediated by the Ebola virus glycoprotein. *J. Virol.* **2006**, *80*, 4174–4178. [[CrossRef](#)]
5. Carette, J.E.; Raaben, M.; Wong, A.C.; Herbert, A.S.; Obernosterer, G.; Mulherkar, N.; Kuehne, A.I.; Kranzusch, P.J.; Griffin, A.M.; Ruthel, G.; et al. Ebola virus entry requires the cholesterol transporter Niemann-Pick C1. *Nature* **2011**, *477*, 340–343. [[CrossRef](#)]
6. Miller, E.; Obernosterer, G.; Raaben, M.; Herbert, A.S.; Deffieu, M.S.; Krishnan, A.; Ndungo, E.; Sandesara, R.G.; Carette, J.E.; Kuehne, A.I.; et al. Ebola virus entry requires the host-programmed recognition of an intracellular receptor. *EMBO J.* **2012**, *31*, 1947–1960. [[CrossRef](#)] [[PubMed](#)]
7. Côté, M.; Misasi, J.; Ren, T.; Bruchez, A.; Lee, K.; Filone, C.; Hensley, L.; Li, Q.; Ory, D.; Chandran, K.; et al. Small molecule inhibitors reveal Niemann-Pick C1 is essential for Ebola virus infection. *Nature* **2011**, *477*, 344–348. [[CrossRef](#)] [[PubMed](#)]
8. Spence, J.S.; Krause, T.B.; Mittler, E.; Jangra, R.K.; Chandran, K. Direct visualization of Ebola virus fusion triggering in the endocytic pathway. *mBio* **2016**, *7*. [[CrossRef](#)]
9. Simmons, J.A.; D’Souza, R.S.; Ruas, M.; Galione, A.; Casanova, J.E.; White, J.M. Ebolavirus glycoprotein directs fusion through NPC1(+) endolysosomes. *J. Virol.* **2016**, *90*, 605–610. [[CrossRef](#)]
10. Saphire, E.; Aman, J.M. Feverish quest for Ebola immunotherapy: Straight or cocktail? *Trends Microbiol.* **2016**, *24*, 684–686. [[CrossRef](#)]
11. Zhao, Y.; Ren, J.; Harlos, K.; Jones, D.M.; Zeltina, A.; Bowden, T.A.; Padilla-Parra, S.; Fry, E.E.; Stuart, D.I. Toremfene interacts with and destabilizes the Ebola virus glycoprotein. *Nature* **2016**, *535*, 169–172. [[CrossRef](#)] [[PubMed](#)]
12. Misasi, J.; Gilman, M.S.; Kanekiyo, M.; Gui, M.; Cagigi, A.; Mulangu, S.; Corti, D.; Ledgerwood, J.E.; Lanzavecchia, A.; Cunningham, J.; et al. Structural and molecular basis for Ebola virus neutralization by protective human antibodies. *Science* **2016**, *351*, 1343–1346. [[CrossRef](#)] [[PubMed](#)]
13. Pallesen, J.; Murin, C.D.; de Val, N.; Cottrell, C.A.; Hastie, K.M.; Turner, H.L.; Fusco, M.L.; Flyak, A.I.; Zeitlin, L.; Crowe, J.E.; et al. Structures of Ebola virus GP and sGP in complex with therapeutic antibodies. *Nat. Microbiol.* **2016**, *1*, 16128. [[CrossRef](#)] [[PubMed](#)]
14. Wang, H.; Shi, Y.; Song, J.; Qi, J.; Lu, G.; Yan, J.; Gao, G.F. Ebola viral glycoprotein bound to its endosomal receptor Niemann-Pick C1. *Cell* **2016**, *164*, 258–268. [[CrossRef](#)]

15. Gong, X.; Qian, H.; Zhou, X.; Wu, J.; Wan, T.; Cao, P.; Huang, W.; Zhao, X.; Wang, X.; Wang, P.; et al. Structural insights into the Niemann-Pick C1 (NPC1)-mediated cholesterol transfer and Ebola infection. *Cell* **2016**, *165*, 1467–1478. [[CrossRef](#)]
16. White, J.M.; Whittaker, G.R. Fusion of enveloped viruses in endosomes. *Traffic* **2016**, *17*, 593–614. [[CrossRef](#)]
17. Weissenhorn, W.; Carfi, A.; Lee, K.-H.; Skehel, J.J.; Wiley, D.C. Crystal structure of the Ebola virus membrane fusion subunit, GP2, from the envelope glycoprotein ectodomain. *Mol. Cell* **1998**, *2*, 605–616. [[CrossRef](#)]
18. Malashkevich, V.N.; Schneider, B.J.; McNally, M.L.; Milhollen, M.A.; Pang, J.X.; Kim, P.S. Core structure of the envelope glycoprotein GP2 from Ebola virus at 1.9-Å resolution. *Proc. Natl. Acad. Sci. USA* **1999**, *96*, 2662–2667. [[CrossRef](#)]
19. Maruyama, T.; Rodriguez, L.; Jahrling, P.; Sanchez, A.; Khan, A.; Nichol, S.; Peters, C.; Parren, P.; Burton, D. Ebola virus can be effectively neutralized by antibody produced in natural human infection. *J. Virol.* **1999**, *73*, 6024–6030. [[CrossRef](#)]
20. Bornholdt, Z.A.; Ndungo, E.; Fusco, M.L.; Bale, S.; Flyak, A.I.; Crowe, J.E.; Chandran, K.; Saphire, E. Host-primed Ebola virus GP exposes a hydrophobic NPC1 receptor-binding pocket, revealing a target for broadly neutralizing antibodies. *mBio* **2015**, *7*. [[CrossRef](#)]
21. Ou, W.; Delisle, J.; Konduru, K.; Bradfute, S.; Radoshitzky, S.R.; Retterer, C.; Kota, K.; Bavari, S.; Kuhn, J.H.; Jahrling, P.B.; et al. Development and characterization of rabbit and mouse antibodies against ebolavirus envelope glycoproteins. *J. Virol. Methods* **2011**, *174*, 99–109. [[CrossRef](#)] [[PubMed](#)]
22. Munro, J.B.; Gorman, J.; Ma, X.; Zhou, Z.; Arthos, J.; Burton, D.R.; Koff, W.C.; Courter, J.R.; Smith, A.B.; Kwong, P.D.; et al. Conformational dynamics of single HIV-1 envelope trimers on the surface of native virions. *Science* **2014**, *346*, 759–763. [[CrossRef](#)] [[PubMed](#)]
23. Das, D.; Govindan, R.; Nikić-Spiegel, I.; Krammer, F.; Lemke, E.A.; Munro, J.B. Direct visualization of the conformational dynamics of single influenza hemagglutinin trimers. *Cell* **2018**, *174*, 926–937. [[CrossRef](#)] [[PubMed](#)]
24. Juette, M.F.; Terry, D.S.; Wasserman, M.R.; Tman, R.; Zhou, Z.; Zhao, H.; Blanchard, S.C. Single-molecule imaging of non-equilibrium molecular ensembles on the millisecond timescale. *Nat. Methods* **2016**, *13*, 341–344. [[CrossRef](#)]
25. Akaike, H. A new look at the statistical model identification. *IEEE Trans. Autom. Control* **1974**, *19*, 716–723. [[CrossRef](#)]
26. Qin, F. Restoration of single-channel currents using the segmental k-means method based on hidden Markov modeling. *Biophys. J.* **2004**, *86*, 1488–1501. [[CrossRef](#)]
27. Zhou, Z.; Cironi, P.; Lin, A.J.; Xu, Y.; Hrvatin, S.; Golan, D.E.; Silver, P.A.; Walsh, C.T.; Yin, J. Genetically encoded short peptide tags for orthogonal protein labeling by Sfp and AcpS phosphopantetheinyl transferases. *ACS Chem. Biol.* **2007**, *2*, 337–346. [[CrossRef](#)]
28. Zhou, Z.; Koglin, A.; Wang, Y.; McMahon, A.P.; Walsh, C.T. An eight residue fragment of an acyl carrier protein suffices for post-translational introduction of fluorescent pantetheinyl arms in protein modification in vitro and in vivo. *J. Am. Chem. Soc.* **2008**, *130*, 9925–9930. [[CrossRef](#)]
29. Corti, D.; Misasi, J.; Mulangu, S.; Stanley, D.A.; Kanekiyo, M.; Wollen, S.; Ploquin, A.; Doria-Rose, N.A.; Staube, R.P.; Bailey, M.; et al. Protective monotherapy against lethal Ebola virus infection by a potently neutralizing antibody. *Science* **2016**, *351*, 1339–1342. [[CrossRef](#)]
30. Shedlock, D.J.; Bailey, M.A.; Popernack, P.M.; Cunningham, J.M.; Burton, D.R.; Sullivan, N.J. Antibody-mediated neutralization of Ebola virus can occur by two distinct mechanisms. *Virology* **2010**, *401*, 228–235. [[CrossRef](#)]
31. Murin, C.D.; Fusco, M.L.; Bornholdt, Z.A.; Qiu, X.; Olinger, G.G.; Zeitlin, L.; Kobinger, G.P.; Ward, A.B.; Saphire, E. Structures of protective antibodies reveal sites of vulnerability on Ebola virus. *Proc. Natl. Acad. Sci. USA* **2014**, *111*, 17182–17187. [[CrossRef](#)] [[PubMed](#)]
32. Qiu, X.; Imonti, J.; Melito, L.P.; Fernando, L.; Ströher, U.; Jones, S.M. Characterization of Zaire ebolavirus glycoprotein-specific monoclonal antibodies. *Clin. Immunol.* **2011**, *141*, 218–227. [[CrossRef](#)] [[PubMed](#)]
33. Wec, A.Z.; Herbert, A.S.; Murin, C.D.; Nyakatura, E.K.; Abelson, D.M.; Fels, M.J.; He, S.; James, R.M.; de Vega, M.-A.; Zhu, W.; et al. Antibodies from a human survivor define sites of vulnerability for broad protection against ebolaviruses. *Cell* **2017**, *169*, 878–890. [[CrossRef](#)]

34. Bornholdt, Z.A.; Turner, H.L.; Murin, C.D.; Li, W.; Sok, D.; Souders, C.A.; Piper, A.E.; Goff, A.; Shamblin, J.D.; Wollen, S.E.; et al. Isolation of potent neutralizing antibodies from a survivor of the 2014 Ebola virus outbreak. *Science* **2016**, *351*, 1078–1083. [[CrossRef](#)]
35. West, B.R.; Wec, A.Z.; Moyer, C.L.; Fusco, M.L.; Ilinykh, P.A.; Huang, K.; Wirchnianski, A.S.; James, R.M.; Herbert, A.S.; Hui, S.; et al. Structural basis of broad ebolavirus neutralization by a human survivor antibody. *Nat. Struct. Mol. Biol.* **2019**, *26*, 204–212. [[CrossRef](#)] [[PubMed](#)]
36. Murin, C.D.; Bruhn, J.F.; Bornholdt, Z.A.; Copps, J.; Stanfield, R.; Ward, A.B. Structural basis of pan-ebolavirus neutralization by an antibody targeting the glycoprotein fusion loop. *Cell Rep.* **2018**, *24*, 2723–2732. [[CrossRef](#)] [[PubMed](#)]
37. Carr, C.M.; Kim, P.S. A spring-loaded mechanism for the conformational change of influenza hemagglutinin. *Cell* **1993**, *73*, 823–832. [[CrossRef](#)]
38. Das, D.; Bulow, U.; Diehl, W.E.; Durham, N.D.; Senjobe, F.; Chandran, K.; Luban, J.; Munro, J.B. Conformational changes in the Ebola virus membrane fusion machine induced by pH, Ca²⁺, and receptor binding. 2019; submitted.
39. Lappala, A.; Nishima, W.; Miner, J.; Fenimore, P.; Fischer, W.; Hraber, P.; Zhang, M.; McMahon, B.; Tung, C.-S. Structural transition and antibody binding of EBOV GP and ZIKV E proteins from pre-fusion to fusion-initiation state. *Biomolecules* **2018**, *8*, 25. [[CrossRef](#)]
40. Brecher, M.; Schornberg, K.L.; Delos, S.E.; Fusco, M.L.; Saphire, E.; White, J.M. Cathepsin cleavage potentiates the Ebola virus glycoprotein to undergo a subsequent fusion-relevant conformational change. *J. Virol.* **2012**, *86*, 364–372. [[CrossRef](#)]



© 2020 by the authors. Licensee MDPI, Basel, Switzerland. This article is an open access article distributed under the terms and conditions of the Creative Commons Attribution (CC BY) license (<http://creativecommons.org/licenses/by/4.0/>).